# Epithelial Membrane Protein 2 (EMP2) Promotes VEGF-Induced Pathological Neovascularization in Murine Oxygen-Induced Retinopathy

Michel Sun,[1] Madhuri Wadehra,[2,3] David Casero,[2] Meng-Chin Lin,[4] Brian Aguirre,[2] Sachin Parikh,[5] Anna Matynia,[5] Lynn Gordon,[1] and Alison Chu[4]

[1]Department of Ophthalmology, Stein Eye Institute, David Geffen School of Medicine, University of California-Los Angeles, Los Angeles, California, United States
[2]Department of Pathology Lab Medicine, David Geffen School of Medicine, University of California-Los Angeles, Los Angeles, California, United States
[3]Jonsson Comprehensive Cancer, David Geffen School of Medicine, University of California-Los Angeles, Los Angeles, California, United States
[4]Division of Neonatology and Developmental Biology, Department of Pediatrics, David Geffen School of Medicine, University of California-Los Angeles, Los Angeles, California, United States
[5]Laboratory of Ocular and Molecular Biology and Genetics, Jules Stein Institute, University of California-Los Angeles, Los Angeles, California, United States

Correspondence: Alison Chu, Division of Neonatology and Developmental Biology, Department of Pediatrics, David Geffen School of Medicine, University of California-Los Angeles, 10833 LeConte Avenue, MDCC B2-375, Los Angeles, CA 90095, USA; alisonchu@mednet.ucla.edu.

MS and MW contributed equally to the work presented here and should therefore be regarded as equivalent authors.

**Received:** May 29, 2019
**Accepted:** November 7, 2019
**Published:** February 7, 2020

Citation: Sun M, Wadehra M, Casero D, et al. Epithelial membrane protein 2 (EMP2) promotes VEGF-induced pathological neovascularization in murine oxygen-induced retinopathy. *Invest Ophthalmol Vis Sci.* 2020;61(2):3. https://doi.org/10.1167/iovs.61.2.3

**Purpose.** Retinopathy of prematurity (ROP) is a leading cause of childhood blindness. ROP occurs as a consequence of postnatal hyperoxia exposure in premature infants, resulting in vasoproliferation in the retina. The tetraspan protein epithelial membrane protein-2 (EMP2) is highly expressed in the retinal pigment epithelium (RPE) in adults, and it controls vascular endothelial growth factor (VEGF) production in the ARPE-19 cell line. We, therefore, hypothesized that *Emp2* knockout (*Emp2* KO) protects against neovascularization in murine oxygen-induced retinopathy (OIR).

**Methods.** Eyes were obtained from wildtype (WT) and *Emp2* KO mouse pups at P7, P12, P17, and P21 after normoxia or hyperoxia (P7−P12) exposure. Following hyperoxia exposure, RNA sequencing was performed using the retina/choroid layers obtained from WT and *Emp2* KO at P17. Retinal sections from P7, P12, P17, and P21 were evaluated for Emp2, hypoxia-inducible factor 1$\alpha$ (Hif1$\alpha$), and VEGF expression. Whole mount images were generated to assess vaso-obliteration at P12 and neovascularization at P17.

**Results.** *Emp2* KO OIR mice demonstrated a decrease in pathologic neovascularization at P17 compared with WT OIR mice through evaluation of retinal vascular whole mount images. This protection was accompanied by a decrease in Hif1$\alpha$ at P12 and VEGFA expression at P17 in *Emp2* KO animals compared with the WT animals in OIR conditions. Collectively, our results suggest that EMP2 enhances the effects of neovascularization through modulation of angiogenic signaling.

**Conclusions.** The protection of *Emp2* KO mice against pathologic neovascularization through attenuation of HIF and VEGF upregulation in OIR suggests that hypoxia-induced upregulation of EMP2 expression in the neuroretina modulates HIF-mediated neuroretinal VEGF expression.

Keywords: retina, retinopathy of prematurity, epithelial membrane protein 2, neovascularization, vascular endothelial growth factor (VEGF), retinal vasculature, angiogenesis, hypoxia

Retinopathy of prematurity (ROP) is the leading cause of childhood blindness. It occurs exclusively in premature infants who are exposed postnatally to relative hyperoxia, which leads to retinal vaso-obliteration, followed by local hypoxia, which encourages neovascularization.[1] This aberrant neovascularization can lead to retinal detachment and blindness in severe cases of ROP. Currently, the most widely accepted pathomechanisms underlying this process involve signaling of hypoxia-inducible factor 1$\alpha$ (Hif1$\alpha$), which regulates vascular endothelial growth factor (VEGF) expression or repression.[1] Other angiogenic factors that may modulate disease include erythropoietin,[2] omega-3 polyunsaturated fatty acids,[3,4] and insulin growth factor 1.[5] Recently, the role of inflammation has been explored in ROP, including macrophage and leukocyte recruitment,[6,7] complement activation,[8,9] neurovascular crosstalk and neuroinflammation,[10,11] and inflammatory responses secondary to oxidative stress.[12,13]

Current treatment strategies include anti-VEGF injections and laser surgery.[14] Although outcomes are improved with anti-VEGF injections, the systemic and long-term side effects are unknown and are of concern given the ubiquitous nature of VEGF.[15] In ischemic retinopathies such as ROP, current therapies target the late phase of neovascularization, although hypoxia initiates oxidative stress and inflammatory responses that characterize the early phase of ROP.[14] These processes also affect tissue integrity and potentially neuronal function.[16,17] Thus, modulation of the disease process prior to the development of later stages of disease (neovascularization seen after the VEGF surge) is beneficial not only in reducing risk of severe neovascularization and end-stage disease, such as retinal detachment, but also in improving long-term outcomes secondary to attenuation of tissue and neuronal damage.

Epithelial membrane protein 2 (EMP2) is a tetraspan membrane protein that has been associated with a number of functions, including cellular invasion and migration, placental angiogenesis, and embryo implantation.[18–20] In placental development and cancer, where local relative hypoxia and inflammation contribute to aberrant vascularization, EMP2 has been shown to regulate VEGF and influence angiogenesis.[18,21] In the eye, EMP2 expression in the retinal pigment epithelium (RPE) has been shown to be upregulated in proliferative vitreoretinopathy,[22,23] underlying its importance in pathologic human retinal processes. In addition, EMP2 modulation in the retinal pigment epithelial cell line ARPE-19 controls VEGF expression.[24] However, EMP2 expression and function in the developing neonatal retina, either under physiologic or pathologic conditions, has not been described. In this paper, the role of EMP2 in a mouse model of ROP was analyzed in order to determine if it can contribute to neovascularization and serve as a potential target in disease.

Based on its modulation of neoangiogenesis in ocular and neoplastic diseases, we hypothesized that reduction in EMP2 levels may attenuate the severity of ROP. As EMP2 expression in early eye development has not been previously described, this study: (1) evaluates the role of EMP2 in normal eye development and in the pathologic state of oxygen-induced retinopathy (OIR); (2) identifies retinal transcriptomic pathways altered in *Emp2* knockout (KO) compared with wild-type (WT) mice after hyperoxia/hypoxia insult; (3) determines whether the *Emp2* KO may be protective against conditions that lead to aberrant neovascularization in experimental ROP; and (4) establishes the pathways through which EMP2 acts to regulate pathologic vasoproliferation.

## Methods

### Ethical Approval

This study was conducted in accordance with established guidelines and all protocols were approved by the Animal Research Committee of the University of California Los Angeles (UCLA) in accordance with the guidelines set by the National Institutes of Health. Animal studies were conducted in adherence to the Association for Research in Vision and Ophthalmology (ARVO) Statement for the Use of Animals in Ophthalmic and Vision Research. Four *Emp2* KO breeding pairs were obtained from the laboratory of Carmen Williams.[18] These animals contained a floxed EMP2 exon 3 and were created on a C57BL/6 background. Breeding was resumed at UCLA, with experiments initiated using third plus generation breeding pairs. For controls, strain-matched WT C57BL/6 mice were purchased from the UCLA Division of Laboratory and Animal Medicine colony. All mice were housed in 12:12 hour light-dark cycles with ad libitum access to a standard rodent chow diet (Pico Lab Rodent Diet 20, cat #5053; Lab Diet, St. Louis, MO, USA) and water.

### Experimental Model of OIR

OIR was produced in the mouse according to standard published guidelines.[25] Briefly, pups were designated at P0.5 the morning that they were found to be delivered. Mothers were maintained on the standard rodent chow diet, as above, during gestation and during suckling. Litters were culled to eight pups, as per protocol recommendations. Mothers were randomly assigned to normoxia conditions or hyperoxia conditions. For those assigned to hyperoxia, on postnatal day 7, nursing mothers and their pups were subjected to hyperoxia (75% oxygen continuously) for 5 days (P7−P12) by placing them in an airtight chamber (BioSpherix Proox model 360; BioSpherix, Parish, NY, USA). Conditions including humidity, temperature, and the health of the animals were assessed twice daily while in the chamber. On postnatal day 12, the mothers and their pups were removed from the chamber and placed back into room air (21% oxygen). Given the stress of hyperoxia on mothers, pups were fostered to a nursing mother after removal from the chamber.

At the end of the experimental period, mice underwent euthanasia using inhaled isoflurane (5−10 minutes). The tissues of interest were dissected within 5 minutes of death and immediately stored for downstream processing (e.g., frozen in liquid nitrogen and stored at -80°C until RNA extraction, stored in formalin, or processed for imaging). All efforts were made to reduce the number of animals used for experiments and to minimize animal suffering. For each time point, condition, and strain of mice, $n = 6–11$ individual pup eyes were used for analysis, and pups used represented between 3 and 5 different litters for each experimental condition and strain.

### Whole Mount Imaging

Whole mount images were prepared as described in previously published standard guidelines for this model of OIR in the mouse.[25] Briefly, after anesthesia, the ocular globe was enucleated and fixed in 4% paraformaldehyde for $1\frac{1}{2}$ hours. Eyes were washed, and then the retina was dissected under a surgical microscope (Leica S6D). Retina cups were washed with phosphate-buffered saline (PBS), blocked with blocking buffer (20% fetal bovine serum (FBS), 2% goat serum, 0.05% bovine serum albumin (BSA), and 1% Triton X-100 in PBS) for 1 hour, and stained with Alexa594-isolectin GS-IB4 (Invitrogen, Carlsbad, CA, USA) in diluent buffer at 4°C overnight. Retinas were then washed with PBS three times and flat mounted onto slides by making peripheral incisions at 90° intervals to divide the retina into four equal-sized quadrants and mounted with ProLong mounting medium (Invitrogen) and a coverslip placed on top. Images were taken using an AxioCam CCD digital camera (Carl Zeiss) mounted to an inverted epifluorescence microscope (AxioVert 135; Carl Zeiss). Due to the dimensions of retinal whole mounts, four to six images per retina were taken at 4X magnification and stitched together.

### Quantification of Vaso-Obliterative and Neo-Vascularization Phase of ROP

Images obtained from whole mount processing of the mouse retinas were processed in Adobe Photoshop C5. Images taken from P12 pups were quantitated for percentage of the vaso-obliterative (VO) area, and images taken from P17 pups were quantitated for percentage of the neovascular (NV) area, using previously published methods.[25] A scorer masked to the groups performed the quantification, and a second masked scorer performed the same procedures for validation of scoring. Briefly, the total retinal area was first quantified using the Polygonal Lasso Tool to trace the vascular area of the entire retina. The areas of VO were outlined using the Lasso Tool to freeform outline the avascular front. The amount of VO was calculated by dividing the number of pixels in the avascular area by the number of pixels of the whole retinal area. Similarly, the Magic Wand Tool was used, with threshold set at 50 to select areas of neovascularization and quantified as the number of pixels of NV as a percentage of the whole retinal area. Similarly, under normoxia conditions, images taken from P7, P12, P17, and P21 pups were quantified for percentage of NV area using the whole mounts, as described above. The total retinal areas were highlighted using the Polygonal Lasso Tool, with vascularization calculated as pixel density using the Magic Wand Tool. Fold change was calculated relative to neovascularization at P7 as a baseline.

### Immunohistochemistry

For immunohistochemistry, whole eye cups were enucleated, rinsed in PBS, fixed in cold 10% neutral buffered formalin for 24 hours, and then transferred to cold 70% ethanol. Samples were embedded in paraffin and sectioned at 4 µm and stained with hematoxylin and eosin by the Translational Pathology Core Laboratory (TPCL) within the Department of Pathology at UCLA.

Retinal thickness was measured during development. Two to four representative measurements were taken for each section, adjacent to the optic nerve plane. Samples were measured from the inner to the outer limiting membranes. To ensure the validity of analysis, sections were used for quantification only if the retinal architecture represented a vertical section through the retina. For image analysis, a mean retinal thickness was calculated from representative measurements taken across each section. In addition, fold-change retinal thickness was calculated in OIR compared with normoxia after correction for total body weight.

Paraffin-embedded sections were evaluated for VEGF expression, as previously described,[18] using the rabbit polyclonal VEGF (A-20) IgG antibody (cat #sc0152; Santa Cruz Biotechnology, Dallas, TX, USA) at a 1:50 dilution.

In some experiments, eyes were fixed frozen (FF) tissue staining. Eyes were rapidly enucleated from embryonic mice and fixed in 4% paraformaldehyde at room temperature for 1 hour. They were then cryopreserved by submersion in 10% sucrose/PBS for 1 hour followed by 30% sucrose/PBS for 2 hours. Samples were then embedded in O.C.T. medium (Tissue-Plus O.C.T. Compound; Fisher Scientific) and sectioned at a thickness of 4 µm by the TPCL.

For image analysis, images were taken at 40X magnification and staining quantitated across the entire retina using Adobe Photoshop's Color Range function to select sampled positive (brown) staining. The RPE layer was erased using a layer mask, and the positive pixels in the retina were counted using the Histogram function. The average number of pixels was calculated in four independent retinal samples per group and used for statistical analysis.

### RNA In Situ Hybridization and *Emp2, Hif1α, Vegfa* mRNA Expression Quantification

RNAscope (RNAscope 2.5 HD Reagent Kit-RED, cat #322350; Advanced Cell Diagnostics (ACD), Newark, CA, USA) was used to detect *Emp2*, *Hif1α*, and *Vegfa* via in situ hybridization.[26] Formalin-fixed paraffin-embedded (FFPE) or fixed frozen (FF) retina samples (P12 and/or P17) were prepared and pretreated according to the manufacturer's protocol (ACD, 322452-USM for FFPE or TN320434 for FF). The probes used in this study were Mm-Emp2 (cat #466851; ACD), Mm-Hif1α (cat #313821; ACD) and Mm-Vegfa (cat #405131; ACD). After probe hybridization and amplification, as per the manufacturer's protocol (322360-USM; ACD), the slides were imaged as described above.

For image analysis and quantification, images were taken at four separate areas of interest representative of the entire length of each retina (inclusive of peripheral and central areas) at 40X magnification. Positive staining (fuchsia) was quantified in Adobe Photoshop using the Color Range function to select sampled fuchsia staining, and pixels counted using the Histogram function. Average number of pixels/section was calculated for each retinal sample and used for statistical analysis.

### Light Stimulus Testing

We tested for basic functional vision in WT and *Emp2* KO mice using a light stimulus test, as previously described.[27] Briefly, for increasing illumination testing (behavioral assay), naïve mice were allowed to acclimate to a dim testing room for 45 minutes, then administered topical atropine eye drops for dilation and dark-adapted for 10 minutes in individual cages. Mice were exposed to various Lux levels (0−1000) for 3-minute intervals. The 0 Lux test was used as a baseline for calculations. For each Lux level, the time spent in light was measured (in seconds) and an aversion index was calculated by comparing time spent in light to time spent in baseline (0 Lux). Four WT mice and 8 *Emp2* KO mice were assessed.

### RNA Sequencing Libraries and Data Analysis

Frozen retinal tissues were obtained from WT normoxia, *Emp2* KO normoxia, WT hyperoxia, and *Emp2* KO hyperoxia groups at P17 ($n$ = 4/group). Briefly, retinal tissue was manually minced and dissociated using sterile scissors followed by homogenization using the QiaShredder kit (cat #79654; Qiagen, Valencia, CA, USA), and RNA extracted using the Qiagen RNeasy Mini Kit (cat #74104; Qiagen), as per the manufacturer's instructions. Total RNA was quantified and RNA degradation was determined using the RNA Integrity Number (RIN). The RIN ranged from 3 to 7. RNA sequencing and library preparation were performed by the UCLA Technology Center for Genomics and Bioinformatics using the KAPA RNA HyperPrep Kit with RiboErase (cat #KK8561; Roche Sequencing, Pleasanton, CA, USA), according to the manufacturer's instructions. The work flow consisted of rRNA depletion, cDNA generation, end repair to generate blunt ends, A-tailing, adaptor ligation,

Investigative Ophthalmology & Visual Science

and polymerase chain reaction (PCR) amplification. Different adaptors were used for multiplexing samples in one lane. Sequencing was performed on the Illumina HiSeq3000 System for a single-read 50 run. Data quality check was done on Illumina SAV. Demultiplexing was performed with the Illumina Bcl2fastq2 version 2.17 program. The raw data has been deposited into the NCBI's Gene Expression Omnibus (GSE123945).

The STAR ultrafast universal RNA-seq aligner version 2.5.2b[28] was used to align the reads to a genome index that includes both the genome sequence (GRCm38 mouse primary assembly) and the exon/intron structure of known mouse gene models (Gencode M12 genome annotation). Alignment files were used to generate strand-specific, gene-level count summaries with STAR's built-in gene counter. Independent filtering was applied as follows: genes with <1 average count across all samples, count outliers, or low mappability (<50 bp) were filtered out for downstream analysis.[28,29] Expression estimates were computed in units of fragments per kilobase of mappable length and million counts (FPKMs). The table of expression estimates (FPKM) was used as input for *SaVanT*[30] to compute enrichment scores on mouse gene expression signatures (Mouse MOE430 Gene Atlas (in the public domain http://www.biogps.org/), Immgen immunological signatures (in the public domain https://www.immgen.org/), hallmark gene sets (in the public domain http://software.broadinstitute.org/gsea), and relative expression profiles. Non-default parameters for *SaVanT* were "*Convert matrix values to ranks*" and "*Compute null distribution with 10000 iterations*." Differential expression analyses were performed with *DESeq2* (Bioconductor, version 3.7, RRID:SCR_015687).[31] Principal component analysis (PCA; S2) was performed with the function *prcomp* in R (in the public domain https://www.R-project.org/) using variance-stabilized data from DESeq2 as input. Count data was fitted to additive models using *Genotype* (WT/MT) and *Condition* (normoxia/hyperoxia) as explanatory factors. The individual effect of each factor on the expression of each gene was tested using a contrast with reduced models (likelihood ratio test). Additional models, including a Genotype:Condition interaction term, were used to fit the data and identify genes with a genotype-specific response to hypoxia. Pairwise differential expression was performed to classify genes as differentially expressed (Wald adjusted $P$ value $< 0.05$) between normoxic and hyperoxic samples in each background. Unfiltered differential expression results are provided in Supplementary Table S1. Functional enrichment of genes expressed between hyperoxia and normoxia groups in both WT and KO mice was performed with Metascape (in the public domain http://www.metascape.org),[32] and significant mouse ontology and pathway terms were compiled. Genes annotated in each functional category were used to estimate average per-genotype effect sizes (fold changes), for up- and down-regulated genes separately. All figures were generated in Matlab (MATLAB, version release 2017a, The MathWorks, Inc., RRID:SCR_001622).

### Quantitative Real-Time Polymerase Chain Reaction

For real-time polymerase chain reaction (RT-PCR) analysis, total cellular RNAs were isolated using the RNeasy Mini kit (cat #74104; Qiagen), following the manufacturers' instructions. Quantitative and qualitative analyses of isolated RNA were assessed by the ratio of absorbance at 260 and 280 nm. The cDNA was generated using 1 µg total RNA using the First-Strand Synthesis SuperMix for quantitative RT-PCR (qRT-PCR) kit (cat #11752050; Invitrogen), according to the manufacturer's instructions. The reverse transcription was performed at 50°C using 50 ng/µl of random hexamers. RT-PCR amplification was performed in triplicate using SybrFast-based detection (cat #07959494001; Kapa), according to the manufacturer's instructions on a LightCycler 480 (Roche, Indianapolis, IN, USA). HIF1-$\alpha$ (primer 1: 5′-GCTCACCATCAGTTATTTACGTG-3′ and primer 2: 5′-CCGTCATCTGTTAGCACCAT-3′) and GAPDH (primer 1: 5′-AATGGTGAAGGTCGGTGTG-3′ and primer 2: 5′-GTGGAGTCATACTGGAACATGTAG-3′) primers were made through Integrated DNA Technologies (Coralville, IA, USA) and lyophilized to 100 uM in nuclease-free water. Relative gene expression was calculated using the comparative CT method with glyceraldehyde 3-phosphate dehydrogenase (GAPDH) expression used as the internal control for normalization. The amplification cycles consisted of: 50°C for 2 minutes, 95°C for 20 seconds, and then 45 cycles of 95°C for 1 second (denaturation), annealing for 20 seconds.

### Statistical Analysis

For all other data except RNA sequencing data, statistical analyses described were conducted in GraphPad Prism software (version 5, GraphPad Software Inc., La Jolla, CA, USA) and data are presented as means ± SEM when data are normally distributed, unless otherwise indicated. Normality was tested for each quantitative dataset using the Shapiro-Wilks normality test. All datasets passed normality testing. To test for significant differences between two groups (WT and *Emp2* KO) for normally distributed data (fold-change of VO and NV), we analyzed results using the Student's *t*-test for parametric data with Welch's correction. When comparing differences between more than two groups (WT and *Emp2* KO normoxia and hyperoxia), we utilized 2-way ANOVA testing and Sidak's multiple comparison testing to distinguish effect by condition (WT versus *Emp2* and normoxia versus hyperoxia). All $P$ values are reported as two-tailed with statistical significance set at $<0.05$ for all comparisons.

Sample sizes for groups were based upon previously published recommendations for this experimental model[25] to evaluate retinal vascular changes, with eyes from 6 to 11 pups obtained for each time point, condition (normoxia and hyperoxia), and strain of mice (WT and *Emp2* KO) representing three to five different litters per condition and strain. Anticipating a 10% change in neovascularization, with an SD of 5%, a sample size of 6 was used as it provided a 98% power with alpha error $<0.05$.

## Results

### EMP2 is Not Essential for Normal Eye Development, Retinal Vascularization, or Light Sensitivity in the Mouse

Previous studies have shown that EMP2 resides in multiple layers of the murine and human eye.[33] Specifically, in the adult retina, EMP2 expression has been shown to reside in the RPE.[24] To determine if EMP2 is required for normal

Investigative Ophthalmology & Visual Science

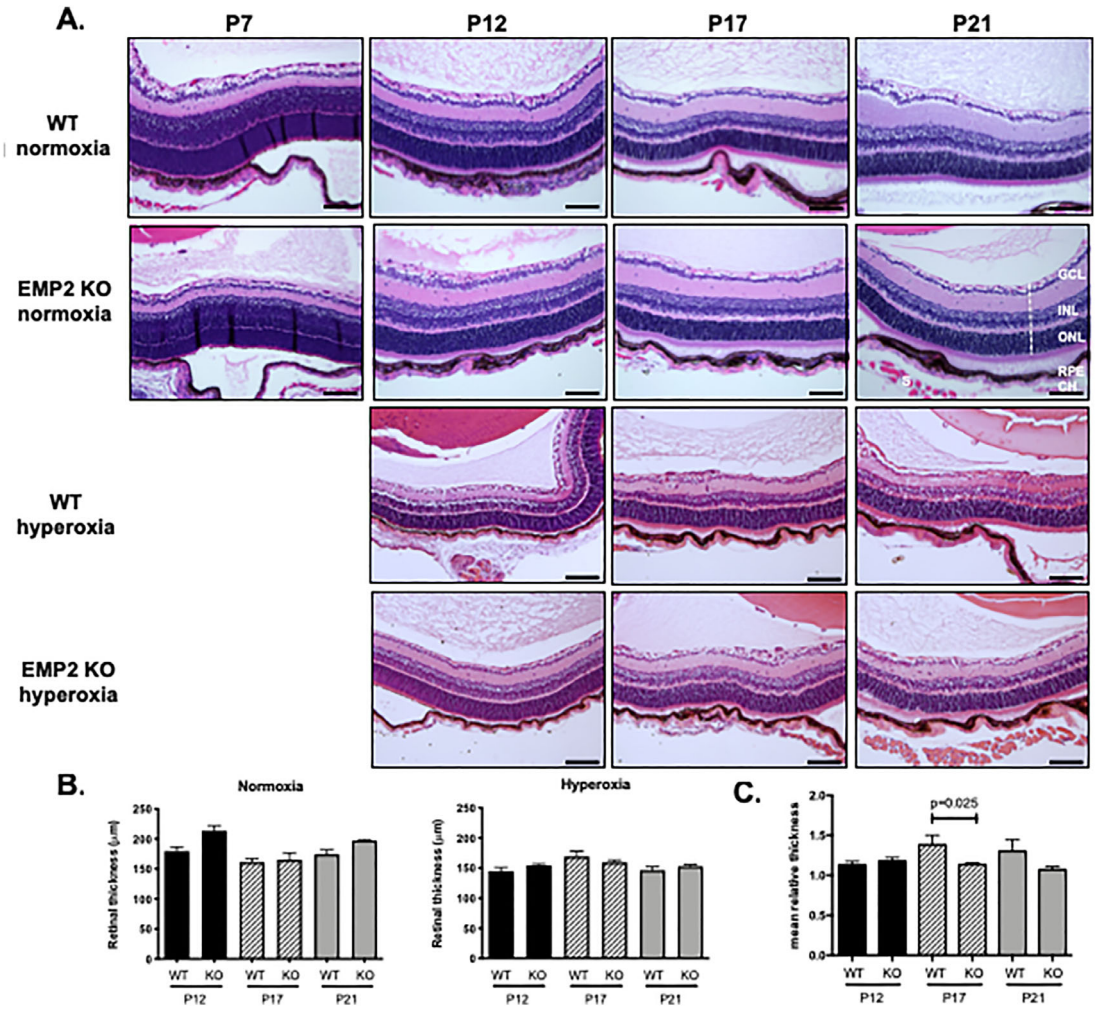


**Figure 1.** KO of *EMP2* does not affect retinal histologic structure. (**A**) WT normoxia (first row), *Emp2* KO normoxia (second row), WT hyperoxia (third row), and *Emp2* KO hyperoxia (fourth row) retinal sections. The dashed line indicates a representative area measured. Hyperoxia treated animals were exposed from P7 to P12, and P7 animals before hyperoxia exposure are not shown. Scale bars represent 100 μM. (**B**) Quantitation of retinal thickness. No differences in retinal thickness between WT and *Emp2* KO mice were observed from quantitation of 20X images at each individual time point (P12, P17, and P21). Data are presented as the mean ± SEM ($N = 6–9$ per group). (**C**) Retinal thickness corrected for body weight in OIR was normalized relative to normoxia retinal thickness corrected for body weight at the same gestational age. Decreased retinal thickness was observed in *Emp2* KO mice compared with WT mice at P17 when normalized for body weight ($P = 0.025$ by Student's *t*-test; $N = 4–7$/group). GCL, ganglion cell layer; INL, inner nuclear layer; ONL, outer nuclear layer; RPE, retinal pigment epithelium; CH: choroid; S, sclera.

ocular development, WT and *Emp2* KO eyes were assessed both for histological and functional changes. By gross histology, the eyes from the *Emp2* KO mice were not different from the C57BL6 WT mice. Standard histological evaluation revealed that the composition and thickness of the retinal layers were consistent at all of the time points evaluated—P7, P12, P17, and P21 under normoxic conditions (Fig. 1A, top two rows). Using whole mount imaging, normal retinal vascularization did not grossly appear to be affected by the absence of EMP2 (Fig. 2).

To next determine function, we used behavioral testing for light sensitivity as a proxy for functional vision. A statistical difference between genotype was observed for the time that animals were present in light ($P = 0.03$). However, when each group was normalized for baseline conditions (time at zero lux), both groups exhibited a similar aversion to light (Fig. 3). Taken together, these results suggest that EMP2 plays a nonessential role in normal ocular development and retinal function.

## *Emp2* is Highly Expressed in the Neuroretina After Relative Hypoxia in Murine OIR

Although *Emp2* expression is limited to the RPE in the retina of adult mice under physiologic conditions, its expression in the developing neonatal eye and particularly in disease states is unknown. We used in situ hybridization to detect mRNA expression of *Emp2* in the retina in murine OIR models. Under normal physiologic conditions, *Emp2* expression is largely limited to the RPE, as shown in adults.

Given previous observations that *Emp2* helps regulate ocular neovascularization in proliferative vitreoretinopathy (PVR),[24,34] we evaluated its role in the retinopathy that

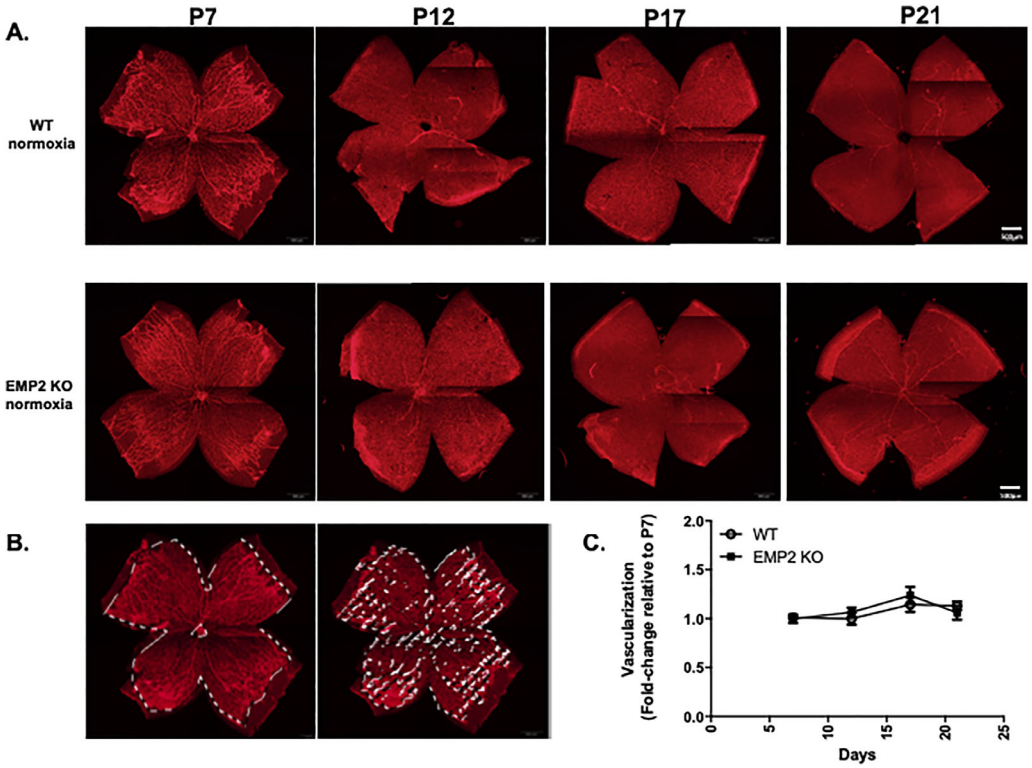


**Figure 2.** *EMP2* KO does not affect retinal vasculature under physiologic conditions. (**A**) Representative whole mount images of retinal vasculature in WT (top row) and *Emp2* KO (bottom row) mice at P7, P12, P17, and P21. Red staining for lectin outlines endothelial cells. Scale bars represent 500 µm. (**B**) Descriptive images outlining areas where pixels highlighting retinal vascularization were quantitated. (**C**) Quantitation of retinal vasculature in whole mount WT and *Emp2* KO mice at P7, P12, P17, and P21. Change in retinal vasculature is calculated at P12, P17, and P21 as fold change of vasculature at P7. Data are presented as the mean ± SEM. No differences were observed between the two groups over time ($P = 0.6$; 2-way ANOVA).

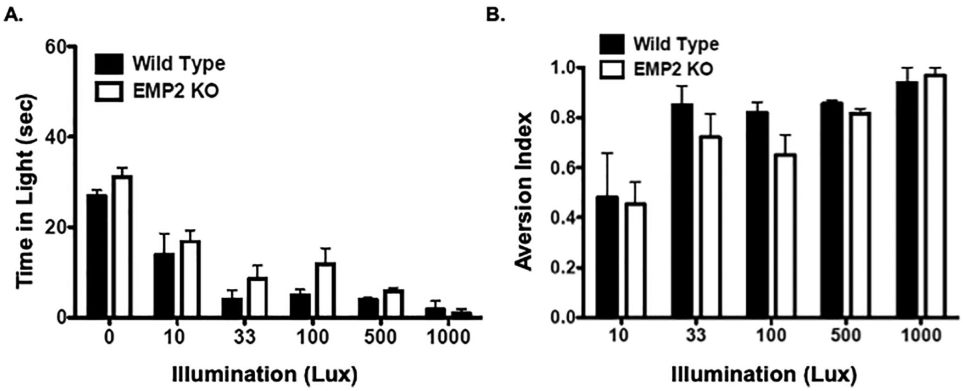


**Figure 3.** *EMP2* KO does not affect light aversion. (**A**) Light aversion assays in WT and *Emp2* KO mice demonstrate that *EMP2* KO mice (open bars) spend more time in the light at various illumination (Lux) levels than WT mice (black bars) ($P = 0.03$) Aversion index is calculated by comparing time spent in light to time spent in baseline (0 Lux). (**B**) Normalization of light aversion indices. When light aversion assay results were normalized to baseline time spent at zero lux, no differences in the aversion index over time were observed between the two groups. Data are represented in graphs as mean ± SEM.

occurs in premature babies. Immediately post-hyperoxia exposure, low levels of EMP2 mRNA were detectable in the neuroretina at P12. However, its expression greatly increased in the neuroretina at P17, the time of peak neovascularization and relative hypoxia (Fig. 4). Specifically, EMP2 mRNA expression was detectable in both the inner and outer neuronal layers as well as lower expression levels in the ganglion cell layer (GCL).

## *Emp2* KO Amplifies the Angiogenic, Inflammatory, and Immune Responses After Hyperoxic Injury

To understand pathogenesis at the disease interface, the retina and choroid were dissected and analyzed using RNA sequencing. We first compared our sequencing data with gene expression signatures from the Mouse Body Atlas

Investigative Ophthalmology & Visual Science

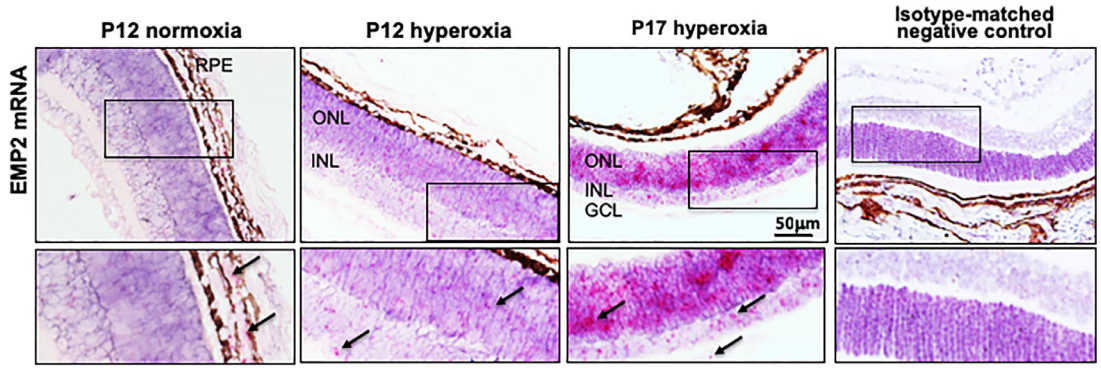


**Figure 4.** EMP2 is expressed in the neuroretina in pathologic OIR. In situ hybridization was used to detect *Emp2* mRNA expression. Representative images of P12 WT mouse pup retinal sections demonstrate *Emp2* mRNA expression within the RPE layer in normoxia conditions. However, in OIR mice, *Emp2* mRNA expression is detected at P12, now in the ONL and INL of the neuroretina, and its expression increased at P17 (peak neovascularization). Isotype-matched negative control is shown for comparison. Scale bars represent 50 µm in the top row. Arrows indicate positive staining (fuchsia) in inset boxes shown in the bottom row. GCL, ganglion cell layer.

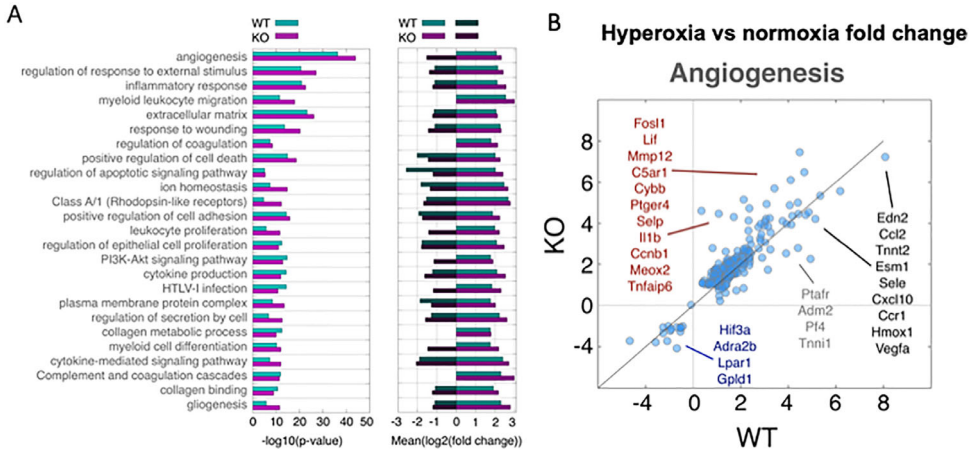


**Figure 5.** Murine OIR results in altered transcriptomic responses between *Emp2* KO and WT mice. (**A**) Left: Functional enrichment of genes differentially expressed after OIR in WT (aqua bars) and *Emp2* KO (fuchsia bars) mice. Similar functional shifts were observed in both *Emp2* KO and WT, including differential expression of genes related to angiogenesis, inflammatory responses, and myeloid leukocyte migration. Right: The average fold change of genes in select functional categories is graphically depicted. Genes were selected as significantly up (positive log2 fold change) or down (negative log2 fold change) for each genotype. In most cases, an amplified transcriptional response (higher average fold change) was observed in *Emp2* KO mice. (**B**) Comparison of gene expression fold changes after OIR in WT (*x*-axis) and *Emp2* KO (*y*-axis) mice. Shown are the results for the broad functional category of angiogenesis (groups of ontology terms in **A** with the same gene members). Selected differentially expressed genes that have a significantly amplified response in KO mice (red lettering), significantly decreased response in KO mice (blue lettering), significantly increased response in WT mice (grey lettering) or similar fold change in both WT and *Emp2* KO mice (black lettering) are highlighted.

expression, which confirmed the retinal/neuronal composition of our samples (Supplementary Fig. S1). At baseline normoxic conditions, significant transcriptomic differences were not detected within the retina and choroid between the WT and *Emp2* KO P17 pups. In fact, only two genes showed mild but consistent transcriptional differences (Wald adjusted $P < 0.05$, fold change approximately 2) between the two groups: *Ide* and *Fgfbp3*, which are known to show altered copy number and expression levels between breeders of C57BL/6J mice.[35]

Following hyperoxia/hypoxia exposure, however, significant differences were observed between the two groups. By PCA, significant transcriptional changes occurred in both genotypes following hyperoxia exposure (Supplementary Fig. S2). Functional pathway analysis revealed that the pathways most affected by hyperoxia exposure included angiogenesis, oxidative stress pathways, immune cell recruitment and proliferation, and apoptosis (Fig. 5A). Within these pathways, *Emp2* KO animals displayed an amplified transcriptomic response. We identified approximately 1000 genes differentially expressed between normoxia and hyperoxia conditions in *Emp2* KO, compared with approximately 700 genes in WT mice. Additionally, genes regulated in both genotypes showed an enhanced response (bigger fold changes) in KO mice (Fig. 5; Supplementary Table S1). Given that angiogenesis is a principal pathomechanistic pathway involved in ROP and was the most significantly affected pathway identified, in-depth analysis of the 222 genes included in the "angiogenesis/vasculogenesis" functional category

Investigative Ophthalmology & Visual Science

revealed that there were a number of key angiogenic genes that were differentially expressed in the *Emp2* KO compared to the WT under OIR conditions (Fig. 5B). To evaluate whether transcriptomic reprogramming reflected changes in the response to oxygen, we specifically examined the alterations in expression of genes known to be involved in HIF1A and VEGF activity. Indeed, a number of HIF-regulated hypoxia response genes (*Lif*, *Il1b*),[36,37] were significantly upregulated in our *Emp2* KO mice along with genes involved in VEGF-mediated ocular angiogenesis (*Ptger4*[38]; listed in red in Fig. 5B). In contrast, genes that were more significantly downregulated in our *Emp2* KO mice were involved in VEGF expression, including *Hif3a*,[39] *Adra2b*,[37] and *Lpar1*[40] (listed in blue in Fig. 5B). Consistent with the angiogenesis signature observed in our data, one study using systemic HIF inhibition to attenuate neovascularization in murine OIR showed that a similar subset of genes, including *Tnfaip6*, *Slc16a3*, *Pdk1*, and *Mif* were involved in HIF inhibition.[41] The independent validation of these genes as attenuators of neovascularization suggests high fidelity of our RNA sequencing results. Together, these findings highly suggest gene-environment partition in the pathogenesis of neovascularization after hyperoxia/hypoxia exposure.

### *Emp2* KO Display Altered Neoangiogenesis

With regard to angiogenesis, both the WT and *Emp2* KO animals showed an upregulation in a number of genes functionally associated with this process, including members of the *Hif* and *Vegf* families (Fig. 5B). To characterize the expression of *Hif* and *Vegf-A* in the development of OIR, their levels were assessed by in situ hybridization, qRT-PCR, or immunohistochemistry. As expected, compared with age-matched normoxic controls, *Hif* and *Vegfa* mRNA abundance increased in all neuronal cell layers of the retina, including the retinal ganglion cell (RGC), inner nuclear layer (INL), and outer nuclear layer (ONL) in retinas of WT animals with OIR at P12 and P17 (Figs. 6 and 7). The transcription factor Hif is upstream of VEGF signaling, with Hif upregulation beginning rapidly after exposure to hypoxia.[42–44] Hif expression in our OIR model peaks at P12 after removal of mice from hyperoxia (75% oxygen) and placement into "relative hypoxia" (21% oxygen), with normalization of Hif levels by P17 (Fig. 6). VEGF expression peaks with maximal neovascular disease at P17 (Fig. 7), both later and longer after initial "hypoxia" exposure, consistent with temporal expression patterns for transcriptional regulation.[42–44] Interestingly, in the P12 OIR mice, *Hif* mRNA expression within the retinal neuronal layers was significantly higher in WT animals than in *Emp2* KO animals, as assessed by RNA in situ hybridization (Fig. 6A; $P = 0.0006$) and validated by qRT-PCR (Fig. 6B; $P = 0.01$). In the P12 and P17 OIR mice, *Vegfa* mRNA expression within the RGC as well as the INLs and ONLs was significantly higher in WT animals than in the *Emp2* KO animals with OIR (Fig. 7A; $P = 0.02$ at P12; $P = 0.001$ at P17). To validate these effects, protein abundance of *Vegf-A* was confirmed by immunohistochemistry staining. P12 and P17 *Emp2* KO animals showed decreased *Vegf-A* protein expression within the RGC and INL layers of retinas with OIR compared with WT animals with OIR (Fig. 7B; $P = 0.0002$ at P12 and $P = 0.006$ at P17). In comparison, age-matched animals from both groups maintained in normoxia showed extremely low mRNA levels of HIF and VEGFA.

### *Emp2* KO Attenuates the Neovascularization Phase and Reduces Retinal Edema in OIR

To determine if the changes in *Hif-1a* and *Vegf-A* functionally correlated with a change in neovascularization, WT and *Emp2* KO mice exposed to hyperoxia were evaluated by whole mount imaging at P12 and P17 (Fig. 8). Peak vaso-obliteration was evaluated at P12, with no differences observed between groups ($P = 0.277$ by Student's *t*-test with Welch's correction). In contrast, there was decreased neovascularization at P17 in the *Emp2* KO group ($P = 0.008$ by Student's *t*-test with Welch's correction) (Fig. 8), confirming a role for EMP2 in the regulation of neoangiogenesis in OIR.

Retinal thickness was also examined under OIR conditions (Fig. 1A, third and fourth rows), as retinal swelling due to edema and inflammation is a major characteristic of ROP.[1,6] We did not find a difference between WT and *Emp2* KO mouse retinal thickness at each time point, under normoxia or OIR conditions (Fig. 1B). Of note, OIR-treated pups are significantly smaller, with an average weight of $4.19 \pm 0.133$ grams (g) at P12 and $5.64 \pm 0.118$ g at P17, compared with normoxia pups who average $6.15 \pm 0.243$ g at P12 and $7.06 \pm 0.268$ g at P17 ($P < 0.0001$ at both time points). Due to the significant effect of hyperoxia on postnatal weight gain, which results in a disparity in size between normoxic and OIR pups during the active phase of disease, which is reported in this model,[25] retinal thickness was normalized to whole body weight (Fig. 1B). Interestingly, retinal thickness in hyperoxia-exposed pups was greater than normoxia pups when adjusted for weight. There was a trend for *Emp2* KO being protective in hyperoxic conditions. Given this, when hyperoxic retinal thickness was normalized relative to normoxia retinal thickness at the same gestational age and corrected for total body weight, WT OIR mice were found to have significantly increased fold-change in retinal thickness at the P17 peak disease time point compared with the *Emp2* KO (Fig. 1C). In conclusion, *Emp2* KO seems to protect against aberrant neovascularization, and may also secondarily reduce retinal edema or inflammation.

## Discussion

Retinopathy of prematurity is a disease exclusive to premature infants exposed to relative hyperoxia that leads to aberrant retinal vascularization. Disease etiology is likely complex, as in recent years a number of players, including angiogenic factors, inflammation, immune cell recruitment, and oxidative stress responses, have been linked to the pathogenesis of this disease.[1,45,46] Current therapies such as anti-VEGF injections or laser therapy target late-phase angiogenic factors/vessel production, and have unknown systemic side effects or long-term consequences on visual impairment and neural function in developing neonates.[15,47–49] Newer strategies of prevention or early rescue treatment prior to severe neovascularization would potentially mitigate risk of severe consequences, and reduce the need for treatment with laser surgery. As *Emp2* has been shown to modulate angiogenesis via regulation of *Vegf* and *Hif1α* in placental diseases and tumor growth,[18–21] we hypothesized that it may play a role in the neovascularization seen in ROP. Our results support this conclusion, as there was a significant decrease in neovascularization at P17 in *Emp2* KO compared with WT animals via *Hif1α*-mediated *Vegf-A* downregulation. Reduction in aberrant vascularization may secondarily protect *Emp2* KO animals from retinal edema, a known

Investigative Ophthalmology & Visual Science

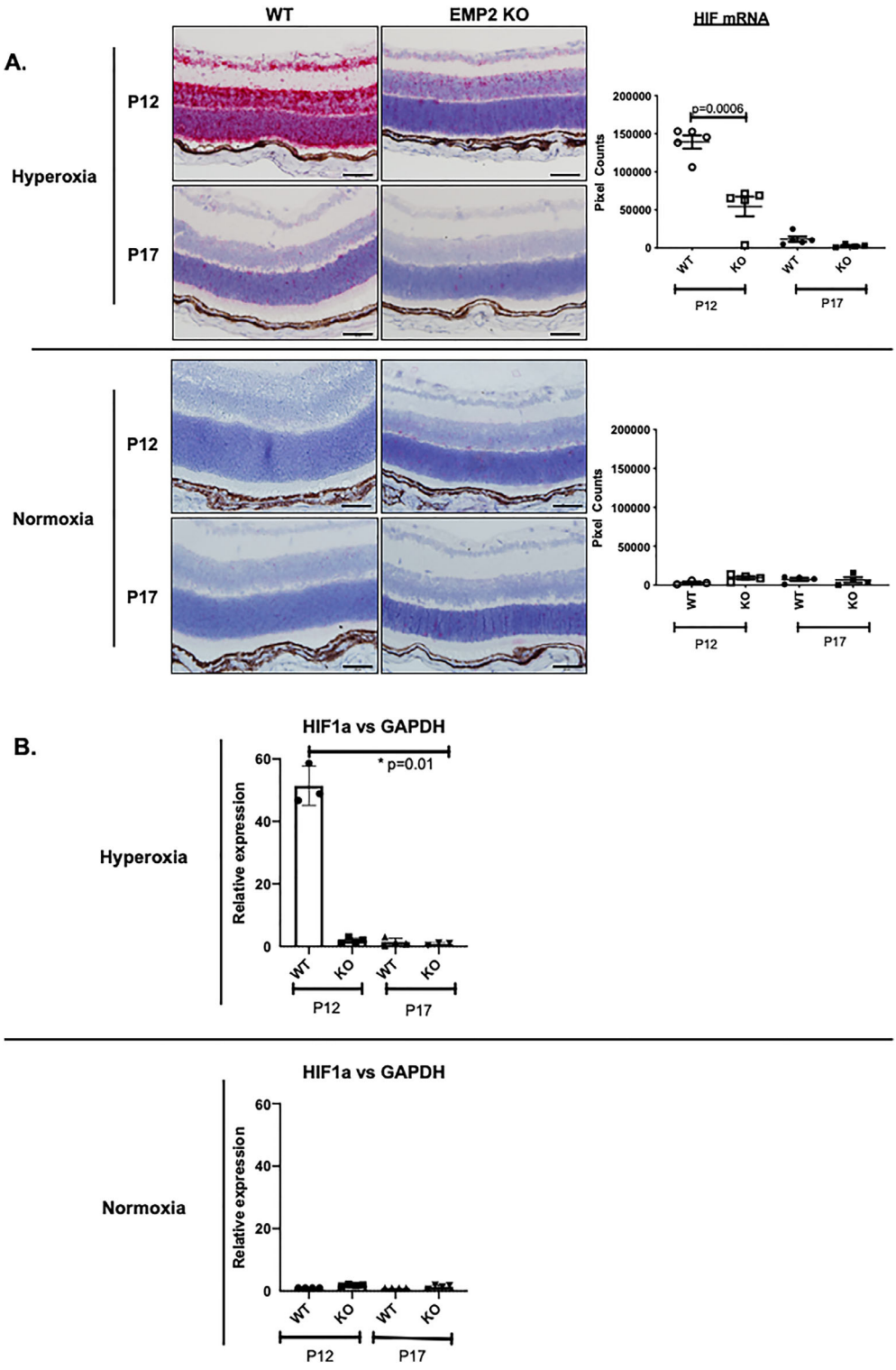


**Figure 6.** WT but not *Emp2* KO mice demonstrate dramatic upregulation of *Hif1α* mRNA expression in retinal neuronal layers in murine OIR at P12. (**A**) Representative images taken using RNA in situ hybridization assays demonstrate high *Hif1α* mRNA expression in OIR conditions in WT but not *Emp2* KO mice at P12 ($P = 0.0006$) (top row). At P17, no significant difference in *Hif1α* mRNA expression is seen between the WT and *Emp2* KO OIR mice (second row). Minimal *Hif1α* mRNA is expressed under normoxic conditions (third and fourth row). Data are graphically summarized as mean average pixel count/area of interest ± SEM ($N = 3–5$ per group). Scale bars represent 50 µm. (**B**) Validation of *Hif1α* mRNA expression in OIR (top graph) and normoxia (bottom graph) conditions by qRT-PCR demonstrates an approximately 50-fold upregulation of *Hif1α* mRNA expression in WT OIR mice at P12 compared with *Emp2* KO OIR mice at P12 as well as both WT and *Emp2* KO OIR mice at P17 ($P = 0.01$). Asterisk indicates $P < 0.05$.

Investigative Ophthalmology & Visual Science

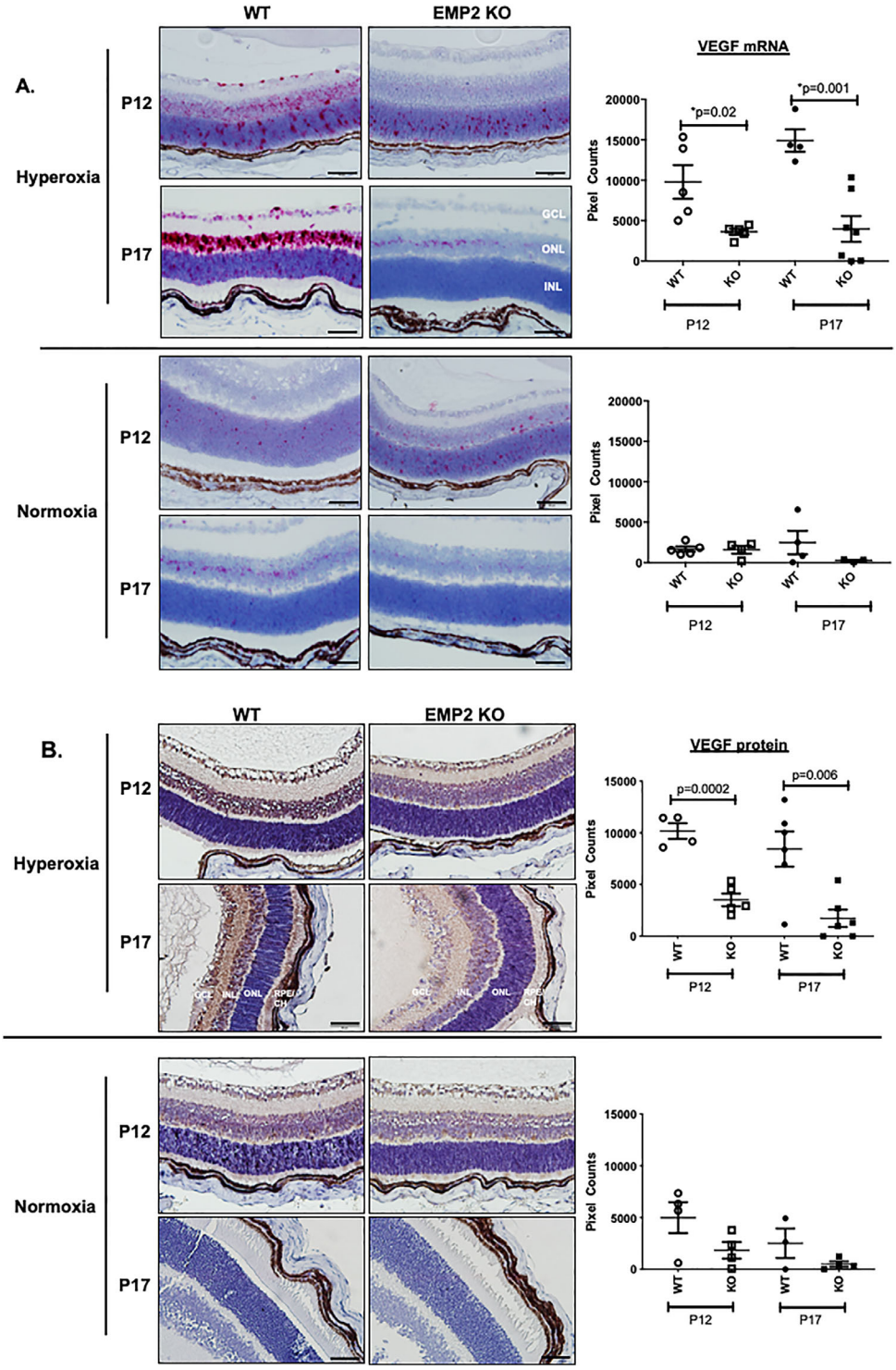


**Figure 7.** WT but not *Emp2* KO mice demonstrate dramatic upregulation of *VEGF* mRNA and protein expression in retinal neuronal layers in murine OIR. (**A**) Representative images taken using RNA in situ hybridization assays demonstrating increased *VegfA* mRNA expression (red staining) in neuronal layers in WT but not *Emp2* KO mice, maximal at P17, 5 days post-hyperoxia exposure ($P = 0.02$ at P12 and $P = 0.001$ at P17 by multiple comparison testing) (top panel). Low *Vegf* mRNA expression was observed in normoxia conditions in both WT and *Emp2* KO mice at P17 (bottom panel). Data are represented in graphs as mean average pixel count/area of interest ± SEM ($N = 4–7$ per group). Scale bars represent 50 µm. (**B**) Representative images taken by immunohistochemistry demonstrating similar patterns of VEGF protein expression (brown) in normoxia and hyperoxia WT and *Emp2* KO mice at P12 and P17. VEGF protein expression increases at P12 and P17 in mice exposed to WT OIR mice compared with *Emp2* KO OIR mice ($P = 0.0002$ and $P = 0.006$, respectively). No significant differences were observed in normoxia groups at P12 or P17. $N = 3$ to 4 per group with data represented as the mean average pixel count ± SEM. Scale bars represent 50 µm. GCL, ganglion cell layer; INL, inner nuclear layer; ONL, outer neuronal layer; RPE, retinal pigment epithelium; CH, choroid.

Investigative Ophthalmology & Visual Science

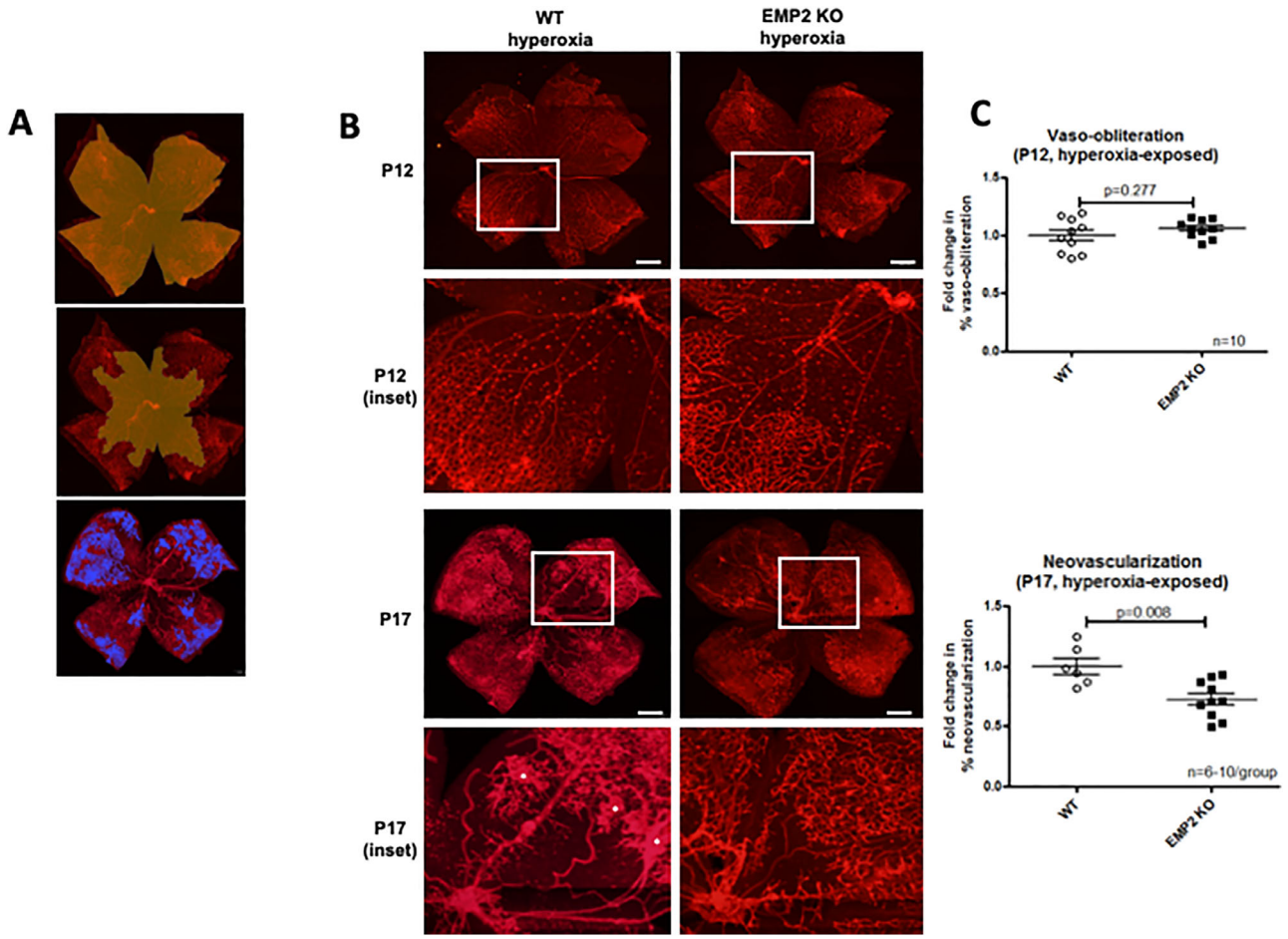


**Figure 8.** *EMP2* KO mice demonstrate attenuated neovascularization at P17 in murine OIR. (**A**) Demonstrative whole mount images depicting how areas for quantification were generated in Photoshop. In the top image, the yellow area represents the area included for calculation of total retinal area. In the middle image, the yellow area represents the area included for calculation of vaso-obliteration. In the bottom image, the blue areas indicate areas of neovascularization. (**B**) Representative whole mount images demonstrating no change in vaso-obliteration at P12 (top row), with enlarged insets (second row), but decreased severity of neovascularization at P17 (third row), with enlarged insets (fourth row) in *Emp2* KO mice (right column) compared with WT mice (left column). Red staining for lectin outlines endothelial cells lining retinal vasculature. Asterisks indicate areas of neovascularization. Scale bars represent 500 µm. (**C**) Graphs representing quantification of vaso-obliteration at P12 (top) showing no difference between WT and *Emp2* KO groups ($P = 0.277$; $N = 10-11$/group), but decreased fold change in neovascularization at P17 (bottom) in *Emp2* KO mice ($P = 0.008$; $N = 6-10$/group). Data are represented in graphs as mean ± SEM.

complication of ROP thought to be due to increased permeability of abnormal neovessels or inflammatory changes leading to capillary permeability and breakdown of the blood retinal barrier.

High levels of EMP2 protein have been previously reported to be present in both the corneal epithelium and RPE in adult mice,[33] with no expression reported within the neuroretina. Here, we demonstrate that genetic KO of *Emp2* had minimal effect on ocular development in the mouse, with histologically normal eye structures and retinal vessel development. Functional vision, as extrapolated from light sensitivity testing, was similarly not altered in *Emp2* KO mice, suggesting that *Emp2* is not necessary for normal ocular function. However, increased expression of *Emp2* was observed in the disease phases of OIR. Our study is the first to show aberrant *Emp2* expression within the neuroretina, largely in the INL and ONL, under pathologic conditions of OIR. This significant upregulation of *Emp2* expression is seen at P17 after the relative hypoxia phase of OIR, but not at P12 (after hyperoxia exposure in OIR), which is consistent with previous studies in other animal and in vitro models demonstrating that *Emp2* upregulation occurs in response to hypoxia.[18,21–24] Taken together, this suggests that EMP2, although not essential for normal retinal development or function under physiologic conditions, does play a role under pathologic conditions, particularly in response to hypoxia.

The question of how mechanistically EMP2 contributes to disease pathogenesis remains unanswered, although its role may be explained through several intriguing possibilities. Previous studies in cancer models have suggested that EMP2 can regulate HIF-1a expression, which would be consistent with our results showing that *Hif-1a* mRNA and protein expression is increased at P12, preceding peak of vasoproliferation and Vegf-A expression at P17.[21] Therefore, direct regulation of angiogenic factor production via EMP2 modulation remains the most plausible mechanism.

HIF-1 is a key transcription factor that plays a major role in ROP disease pathogenesis[50] by mediating expression of hypoxia-regulated genes, including VEGF. The role of HIF

Investigative Ophthalmology & Visual Science

as a master oxygen sensor and driver of neovascularization in diseases such as diabetic retinopathy, retinal vein occlusions, and ROP has been well documented.[51,52] Astrocytes, glia, Müller cells, and neurons such as ganglion cells, as well as the RPE/choroid layer have all been shown to produce or respond to increased VEGF.[53,54] Consistent with many of these studies, our investigation showed that HIF and VEGF mRNA and protein were enhanced at the height of hyperoxic (P12) or hypoxic (P17) exposure, respectively, especially in the neuroretina. EMP2 in this model may be acting through modulation of the HIF-mediated angiogenic cascade, a mechanism that is supported by the established role of EMP2 in cancer models.[20,21] HIF-1*a* interacts with many protein factors, and its stability is regulated by various post-translational modifications, hydroxylation, acetylation, and phosphorylation. HIF-1*a* protein stability is determined by a complex balance of many factors, such as oxygen-dependent ubiquitination, and negative and positive regulators, including various oxygen independent factors such as growth factor signaling.[43] EMP2, an established angiogenic player, may reasonably also modulate activity through this intricate network, although the temporal relationship of its interactions needs further investigation. Future studies will also be focused on characterizing *Emp2*, *Hif-1a*, and *Vegf-A* interactions between the different cell populations within the neuroretina.

RNA sequencing of whole retinal samples was performed in order to further identify potential protective interactions in the *Emp2* KO mice that explain their significant attenuation of neovascularization. First, the overall transcriptomic data are consistent with several reports in the literature that ROP pathology is the result of several interacting aberrant responses in angiogenesis, inflammatory, immune response, and oxidative stress pathways,[6–9,11–14,45,46] and these pathways were similarly represented in this model as differentially expressed for age-matched mice exposed to normoxic versus OIR conditions. To our knowledge, our RNA sequencing data is among the first transcriptomic databases in the murine OIR model and can potentially be mined to identify novel pathways.

Our retinal transcriptomic data highlights that the pathway that is most highly altered in OIR is in angiogenesis. Of the HIF protein family members, Hif-1a, which was a major focus of our study, was not identified as being highly differentially expressed in the RNA sequencing data. This is likely because the expected peak expression of Hif-1a is at P12 (Fig. 6), whereas the RNA sequencing was performed at peak neovascularization of P17, so any transient change in transcript expression may have been earlier than the time point chosen for our RNA sequencing data. Additionally, regulation of HIF-1*a* protein is primarily at the level of ubiquitination and post-translational modification, with possibly less variability in transcript at the P17 represented time point. A related isoform, Hif-3*a*, was noted to be downregulated in the *EMP2* KO mice under OIR conditions at P17 (Fig. 5B, blue). HIF-3*a* lacks the transcriptional activation domain present in HIF-1*a* and HIF-2*a*, and as such is thought to act as a dominant negative regulator of HIF-1.[43] HIF3*a* mRNA levels are more responsive to hypoxia than either HIF-1 or HIF-2,[55] but may have a different temporal expression pattern, and further study at the earlier P12 time point when maximal HIF-1*a* expression is expected could be informative.

Another prominent pathway implicated by the RNA sequencing data is the inflammatory response pathway. Interestingly, almost all of the significantly differentially upregulated genes (Fig. 5B, red) in the *EMP2* KO mice under OIR were immune related, including C5ar1 (complement C5a receptor 1), Il1b (interleukin 1 beta), Lif (leukemia inhibitor factor), Tnfaip6 (tumor necrosis factor inducible protein 6), Cybb (cytochrome b-245, beta chain, member of the NADPH oxidase complex), Ptger4 (prostaglandin E receptor 4), and Selp (selectin P). It is possible that EMP2 may indirectly regulate RPE function by altering immune or inflammatory responses.[56–58] Although RNA sequencing results suggest that this is possible, no obvious histological inflammation was observed, and the significance of these findings remain to be clarified.

This study has demonstrated that *EMP2* KO protects against aberrant neovascularization, and suggests that knockdown of EMP2 may be a novel and safe target by which disease severity could be modulated. Given that progressive fibrovascular contraction and tractional retinal detachment has been shown to occur in up to 50% of patients following anti-VEGF injections for retinopathy of prematurity,[59] a need remains to find novel therapeutic targets. EMP2 may be a more specific target for ocular neovascular diseases, as it is expressed in the corneal epithelium and RPE in the eye, with potential for fewer off-target effects. Additionally, targeting EMP2 seems to be safe in developing neonates, with no measurable effect on visual function. Future studies will be directed toward understanding the mechanisms by which EMP2 modulates VEGF expression, and toward determining the potential benefits and risks of anti-EMP2 based therapies.

## *Acknowledgments*

The authors thank Christie Qin for her assistance in this work. We also thank Ann Chan for her technical help in sample preparation.

Supported by the Little Giraffe Foundation (AC), by K08 HD093874 (AC), by NIH/NCI P50-CA211015 (MW) and NCI R01 CA163971 (MW). This work is also supported by an Unrestricted Grant from Research to Prevent Blindness, Inc., to the Department of Ophthalmology at UCLA. The content is solely the responsibility of the authors and does not necessarily represent the official view of the National Institutes of Health.

Disclosure: **M. Sun**, None; **M. Wadehra**, None; **D. Casero**, None; **M.-C. Lin**, None; **B. Aguirre**, None; **S. Parikh**, None; **A. Matynia**, None; **L. Gordon**, None; **A. Chu**, None

## *References*

1. Rivera JC, Sapieha P, Joyal JS, et al. Understanding retinopathy of prematurity: update on pathogenesis. *Neonatology*. 2011;100:343–353.
2. Chen J, Connor KM, Aderman CM, Smith LE. Erythropoietin deficiency decreases vascular stability in mice. *J Clin Invest*. 2008;118:526–533.
3. Pawlik D, Lauterbach R, Walczak M, Hurkala J, Sherman MP. Fish-oil fat emulsion supplementation reduced the risk of retinopathy in very low birth weight infants: a prospective, randomized study. *JPEN J Parenter Enteral Nutr*. 2014;38:711–716.
4. Connor KM, SanGiovanni JP, Lofqvist C, et al. Increased dietary intake of omega-3-polyunsaturated fatty acids reduces pathological retinal angiogenesis. *Nat Med*. 2007;13:868–873.

5. Lofqvist C, Willett KL, Aspergren O, et al. Quantification and localization of the IFG/insulin system expression in retinal blood vessels and neurons during oxygen-induced retinopathy in mice. *Invest Ophthalmol Vis Sci.* 2009;50:1831–1837.
6. Rathi S, Jalali S, Patnaik S, et al. Abnormal complement activation and inflammation in the pathogenesis of retinopathy of prematurity. *Front Immunol.* 2017;8:1868.
7. Ishida S, Yamashiro K, Usui T, et al. Leukocytes mediate retinal vascular remodeling during development and vaso-obliteration in disease. *Nat Med.* 2003;9:781–788.
8. Sweigard JH, Yanai R, Gaissert P, et al. The alternative complement pathway regulates pathological angiogenesis in the retina. *FASEB J.* 2014;28:3171–3182.
9. Langer HF, Chung KJ, Orlova VV, et al. Complement-mediated inhibition of neovascularization reveals a point of convergence between innate immunity and angiogenesis. *Blood.* 2010;116: 4395–4403.
10. Dorrell MI, Aguilar E, Jacobson R, et al. Maintaining retinal astrocytes normalizes revascularization and prevents vascular pathology associated with oxygen-induced retinopathy. *Glia.* 2010;58:43–54.
11. Liu X, Wang D, Liu Y, et al. Neuronal-driven angiogenesis: role of NGF in retinal neovascularization in an oxygen-induced retinopathy model. *Invest Ophthalmol Vis Sci.* 2010;51:3749–3757.
12. Saito Y, Geisen P, Uppal A, Hartnett ME. Inhibition of NAD(P)H oxidase reduces apoptosis and avascular retina in an animal model of retinopathy of prematurity. *Mol Vis.* 2007;13:840–853.
13. Wang H, Zhang SX, Hartnett ME. Signaling pathways triggered by oxidative stress that mediate features of severe retinopathy of prematurity. *JAMA Ophthalmol.* 2013;131:80–85.
14. Rivera JC, Dabouz R, Noueihed B, Omri S, Tahiri H, Chemtob S. Ischemic retinopathies: oxidative stress and inflammation. *Oxid Med Cell Longev.* 2017;2017:3940241.
15. Khalili S, Shifrin Y, Pan J, Belik J, Mireskandari K. The effect of a single anti-vascular endothelial growth factor injection on neonatal growth and organ development: in-vivo study. *Exp Eye Res.* 2018;169:54–59.
16. Vessey KA, Wilkinson-Berka JL, Fletcher EL. Characterization of retinal function and glial cell response in a mouse model of oxygen-induced retinopathy. *J Comp Neurol.* 2011;519:506–527.
17. Mehdi MK, Sage-Ciocca D, Challet E, Malan A, Hicks D. Oxygen-induced retinopathy induces short-term glial stress and long-term impairment of photoentrainment in mice. *Graefes Arch Clin Exp Ophthalmol.* 2014;252: 595–608.
18. Williams CJ, Chu A, Jefferson WN, et al. Epithelial membrane protein 2 (EMP2) deficiency alters placental angiogenesis, mimicking features of human placental insufficiency. *J Pathol.* 2017;242:246–259.
19. Wadehra M, Dayal M, Mainigi M, et al. Knockdown of the tetraspan protein epithelial membrane protein-2 inhibits implantation in the mouse. *Dev Biol.* 2006;292:430–441.
20. Fu M, Rao R, Sudhakar D, et al. Epithelial membrane protein-2 promotes endometrial tumor formation through activation of FAK and Src. *PLoS One.* 2011;6:e19945.
21. Gordon LK, Kiyohara M, Fu M, et al. EMP2 regulates angiogenesis in endometrial cancer cells through induction of VEGF. *Oncogene.* 2013;32:5369–5376.
22. Telander DG, Yu AK, Forward KI, et al. Epithelial membrane protein -2 in human proliferative vitreoretinopathy and epiretinal membranes. *Invest Ophthalmol Vis Sci.* 2016;57:3112–3117.
23. Telander DG, Morales SA, Mareninov S, Forward K, Gordon LK. Epithelial membrane protein-2 (EMP2) and experimental proliferative vitreoretinopathy (PVR). *Curr Eye Res.* 2011;36:546–552.
24. Morales SA, Telander DG, Leon D, et al. Epithelial membrane protein 2 controls VEGF expression in ARPE-19 cells. *Invest Ophthalmol Vis Sci.* 2013;54:2367–2372.
25. Connor KM, Krah NM, Dennison RJ, et al. Quantification of oxygen-induced retinopathy in the mouse: a model of vessel loss, vessel regrowth and pathological angiogenesis. *Nat Protoc.* 2009;4:1565–1573.
26. Wang F, Flanagan J, Su N, et al. RNAscope: a novel in situ RNA analysis platform for formalin-fixed, paraffin-embedded tissues. *J Mol Diagn.* 2012;14:22–29.
27. Qin Y, Chan AM, Chang YL, et al. Human embryonic stem cell-derived mesenchymal stromal cells decrease the development of severe experimental autoimmune uveitis in B10.RIII mice. *Ocul Immunol Inflamm.* 2018;26:1228–1236.
28. Dobin A, Davis CA, Schlesinger F, et al. STAR: ultrafast universal RNA-seq aligner. *Bioinformatics.* 2013;29:15–21.
29. Casero D, Sandoval S, Seet CS, et al. Long non-coding RNA profiling of human lymphoid progenitor cells reveals transcriptional divergence of B cell and T cell lineages. *Nat Immunol.* 2015;16:1282–1291.
30. Lopez D, Montoya D, Ambrose M, et al. SaVanT: a web-based tool for the sample-level visualization of molecular signatures in gene expression profiles. *BMC Genomics.* 2017;18:824.
31. Love MI, Huber W, Anders S. Moderated estimation of fold change and dispersion for RNA-seq data with DESeq2. *Genome Biol.* 2014;15:550.
32. Zhou Y, Zhou B, Pache L, et al. Metascape provides a biologist-oriented resource for analysis of systems-level datasets. *Nat Commun.* 2019;10:1523.
33. Wadehra M, Sulur GG, Braun J, Gordon LK, Goodglick L. Epithelial membrane protein-2 is expressed in discrete anatomical regions of the eye. *Exp Mol Pathol.* 2003;74:106–112.
34. Morales SA, Mareninov S, Wadehra M, et al. FAK activation and the role of epithelial membrane protein 2 (EMP2) in collagen gel contraction. *Invest Ophthalmol Vis Sci.* 2009;50:462–469.
35. Watkins-Chow DE, Pavan WJ. Genomic copy number and expression variation within the C57BL/6J inbred mouse strain. *Genome Res.* 2008;18:60–66.
36. Wu L, Yu H, Zhao Y, et al. HIF-2$\alpha$ mediates hypoxia-induced LIF expression in human colorectal cancer cells. *Oncotarget.* 2015;6:4406–4417.
37. Watanabe K, Zhang XY, Kitagawa K, Yunoki T, Hayashi A. The effect of clonidine of VEGF expression in human retinal pigment epithelial cells (ARPE-19). *Graefes Arch Clin Exp Ophthalmol.* 2009;247:207–213.
38. Yanni SE, Barnett JM, Clark ML, Penn JS. The role of PGE2 receptor EP4 in pathologic ocular angiogenesis. *Invest Ophthalmol Vis Sci.* 2009;50:5479–5486.
39. D'Amico AG, Maugeri G, Rasà DM, et al. NAP counteracts hyperglycemia/hypoxia induced retinal pigment epithelial barrier breakdown through modulation of HIFs and VEGF expression. *J Cell Physiol.* 2018;233:1120–1128.
40. Kitayoshi M, Fukui R, Tanabe E, et al. Different effects on cell proliferation and migration abilities of endothelial cells by $LPA_1$ and $LPA_3$ in mammary tumor FM3A cells. *J Recept Signal Transduct Res.* 2012;32:209–213.
41. Hoppe G, Yoon S, Gopalan B, et al. Comparative systems pharmacology of HIF stabilization in the prevention of retinopathy of prematurity. *Proc Natl Acad Sci USA.* 2016;113:E2516–E2525.
42. Dengler VL, Galbraith M, Espinosa JM. Transcriptional regulation by hypoxia inducible factors. *Crit Rev Biochem Mol Biol.* 2014;49:1–15.


Investigative Ophthalmology & Visual Science

43. Lee JW, Bae SH, Jeong JW, et al. Hypoxia-inducible factor (HIF-1) alpha: its protein stability and biological functions. *Exp Mol Med.* 2004;36:1–12.
44. Ozaki H, Yu AY, Della N, et al. Hypoxia inducible factor-1alpha is increased in ischemic retina: temporal and spatial correlation with VEGF expression. *Invest Opthalmol Vis Sci.* 1999;40:182–189.
45. Hellström A, Smith LE, Dammann O. Retinopathy of prematurity. *Lancet.* 2013;382:1445–1457.
46. Hartnett ME, Penn JS. Mechanisms and management of retinopathy of prematurity. *N Engl J Med.* 2012;367:2515–2526.
47. Sankar MJ, Sankar J, Chandra P. Anti-vascular endothelial growth factor (VEGF) drugs for treatment of retinopathy of prematurity. *Cochrane Database Syst Rev.* 2018;1:CD009734.
48. Hu J, Blair MP, Shapiro MJ, Lichtenstein SJ, Galasso JM, Kapur R. Reactivation of retinopathy of prematurity after bevacizumab injection. *Arch Ophthalmol.* 2012;130:1000–1006.
49. Sato T, Wada K, Arahori H, et al. Serum concentrations of bevacizumab (avastin) and vascular endothelial growth factor in infants with retinopathy of prematurity. *Am J Ophthalmol.* 2012;153:327–333.
50. Peet DJ, Kittipassorn T, Wood JP, Chidlow G, Casson RJ. HIF signalling: the eyes have it. *Exp Cell Res.* 2017;356:136–140.
51. Campochiaro PA. Molecular pathogenesis of retinal and choroidal vascular diseases. *Prog Retin Eye Res.* 2015;49:67–81.
52. Campochiaro PA. Ocular neovascularization. *J Mol Med.* 2013;91:311–321.
53. Zhou TE, Rivera JC, Bhosle VK, et al. Choroidal involution is associated with a progressive degeneration of the outer retinal function in a model of retinopathy of prematurity: early role for IL-1$\beta$. *Am J Pathol.* 2016;186:3100–3116.
54. Hartnett ME. Pathophysiology and mechanisms of severe retinopathy of prematurity. *Ophthalmology.* 2015;122:200–210.
55. Heidbreder M, Fröhlich F, Jöhren O, et al. Hypoxia rapidly activates HIF-3alpha mRNA expression. *FASEB J.* 2003;17:1541–1543.
56. Gao S, Li C, Zhu Y, et al. PEDF mediates pathological neovascularization by regulating macrophage recruitment and polarization in the mouse model of oxygen-induced retinopathy. *Sci Rep.* 2017;7:42846.
57. Zhou Y, Yoshida S, Nakao S, et al. M2 macrophages enhance pathological neovascularization in the mouse model of oxygen-induced retinopathy. *Invest Ophthalmol Vis Sci.* 2015;56:4767–4777.
58. Liyanage SE, Fantin A, Villacampa P, et al. Myeloid-derived vascular endothelial growth factor and hypoxia-inducible factor are dispensable for ocular neovascularization-brief report. *Arterioscler Thromb Vasc Biol.* 2016;36:19–24.
59. Yonekawa Y, Wu WC, Nitulescu CE, et al. Progressive retinal detachment in infants with retinopathy of prematurity treated with intravitreal bevacizumab or ranibizumab. *Retina.* 2018;38:1079–1083.


Investigative Ophthalmology & Visual Science